J. Fluid Mech. (1999), *vol.* 392, *pp.* 27–44. Printed in the United Kingdom

© 1999 Cambridge University Press

The dynamics of sedimenting surface gravity currents

By T. MAXWORTHY†

Institute of Theoretical Geophysics, Department of Applied Mathematics and Theoretical Physics, University of Cambridge, Silver Street, Cambridge, CB3 9EW, UK

(Received 15 August 1997 and in revised form 18 November 1998)

We have performed a series of experiments on the dynamics of sedimenting, surface gravity currents. The physical situation concerns a current, with total density ρ_C, evolving at the surface of a fluid of greater density, ρ_A. In turn ρ_C is made up of interstitial fluid of density ρ_I and heavy particles with a concentration by weight c and a density ρ_P. Only the case of the release of a constant volume of particles and interstitial fluid has been considered in detail. It has been found that the sedimentation of the particles, plus some of the interstitial fluid, through the interface between the two fluids has a profound effect upon the motion of the current. When the rejected mixture of particles and upper- and lower-layer fluids reaches the bottom of the experimental tank it generates a secondary gravity current which in turn interacts with the primary current to further modify its behaviour. Using simple models we have been able to rationalize the observations and reveal the dynamical balances which appear to be important. A subsidiary experiment and analysis on the flux characteristics of the interface have been performed in order to further clarify the important effects of the particle motion through that region.

1. Introduction

The subject of sedimenting gravity currents is an interesting one from a fundamental point of view, and one with a number of important applications. Several experimental/modelling papers have appeared recently, mainly concerned with current propagation over a solid surface. In the earliest work (Bonnecaze, Huppert & Lister 1993) the current was made up of particles and interstitial fluid, with the latter having the same or higher density than the ambient. In this case, the particles, as they fell, were deposited onto the solid surface and no longer took part in the force balance which set the forward motion of the current. In the second case the interstitial fluid was lighter than the ambient (Sparks *et al.* 1993) and as the particles sedimented downwards this lighter fluid was released and moved upwards carrying some particles with it. Simple 'box-models' were found to describe the current motion well, once the loss of particles and concommittent decrease in current density were taken into account. Applications to pyroclastic flows from volcanoes, turbidity currents, etc. were invoked as motivation for working on such problems.

In the present work the motivations are similar. When the dust cloud from a volcanic eruption reaches its level of neutral buoyancy it spreads laterally as an intrusion, the dynamics of which are modified by the flux of particles, and interior

† Permanent Address: Department of Aerospace and Mechanical Engineering, University of Southern California, Los Angeles, CA 90089-1191, USA.

https://doi.org/10.1017/S002211209900556X Published online by Cambridge University Press

fluid, through the bottom interface. The motion at the upper interface has much in common with the flow considered above by Sparks *et al.* (1993), with interior fluid and a few particles convecting upwards. Similarly when a sediment-laden fresh-water riverine outflow reaches the denser ocean it can, depending on its relative density, propagate outwards at any level. Here we consider the case where it is lighter than the surface layers of the ocean and hence will move along that surface, depositing particles and mixing as it travels. The question we ask here, and answer to some degree, is how is the current motion affected by this flux and what unexpected phenomena take place.

The question of the dynamics of such a sedimenting interface has been studied to some extent in the case where there is little or no horizontal velocity in either fluid. Here we refer to Green (1987) and Chen (1997) who noticed the similarity between the convective modes seen in this case and those observed in double-diffusive convection (e.g. Turner 1976). These similarities become even more evident upon comparing the present results with those for double-diffusive gravity currents found in Maxworthy (1983). Many of the same phenomena occur, and while the details are different much of the modelling effort from that work carries over to the present case.

2. Apparatus and experimental procedure

2.1. *Apparatus to study gravity current motion*

The major piece of equipment that evolved during the course of this investigation is shown in figure 1(*a*). It consisted of a rectangular tank 220 cm long, 57 cm deep and 15.7 cm wide. At one end a smaller reservoir was attached that was 10 cm deep and 40 cm long, and its effective length could be varied by inserting barriers at 7.6 cm intervals, while it could be isolated from the main tank by a removable barrier at the open end. It was used to study the motion generated by the release of a fixed volume of interstitial fluid plus particles.

At the start of an experiment the main tank was filled with a dense solution of sodium chloride in water, the density (ρ_A) of which was measured to five decimal places using a specific gravity bottle calibrated against pure water. The secondary box was filled with a well-mixed and known volume of particle-laden interstitial fluid, e.g. fresh water, that had been prepared by adding an accurately weighed mass of particles (m_P) to an accurately known weight of fluid (m_I). The particle concentration by weight (c) was given by

$$c = m_P/(m_P + m_I),$$

so that the density of the mixture (ρ_C) could be calculated using

$$1/\rho_C = (c/\rho_P) + (1 - c)/\rho_I \tag{1}$$

or, upon rearranging,

$$\rho_C = \rho_I/(1 - ck) \quad \text{or} \quad \rho_C - \rho_I = \rho_I\, ck/(1 - ck), \tag{2}$$

where ρ_I is the density of the interstitial fluid, ρ_P that of the particles and $k = 1-(\rho_I/\rho_P)$. For the particles used here $\rho_P = 3.217\,\mathrm{g\,cm^{-3}}$ so that $k = 0.6897$ for these particles suspended in pure water at 20 °C. Of course the physical characteristics of the particles themselves were also important, in particular their number and weight distributions with diameter. Here we used 1000 grade carborundum powder, the characteristics of which are discussed in detail in § 3.1.

To start the fluid dynamical component of an experiment the mixture in the

https://doi.org/10.1017/S002211209900556X Published online by Cambridge University Press

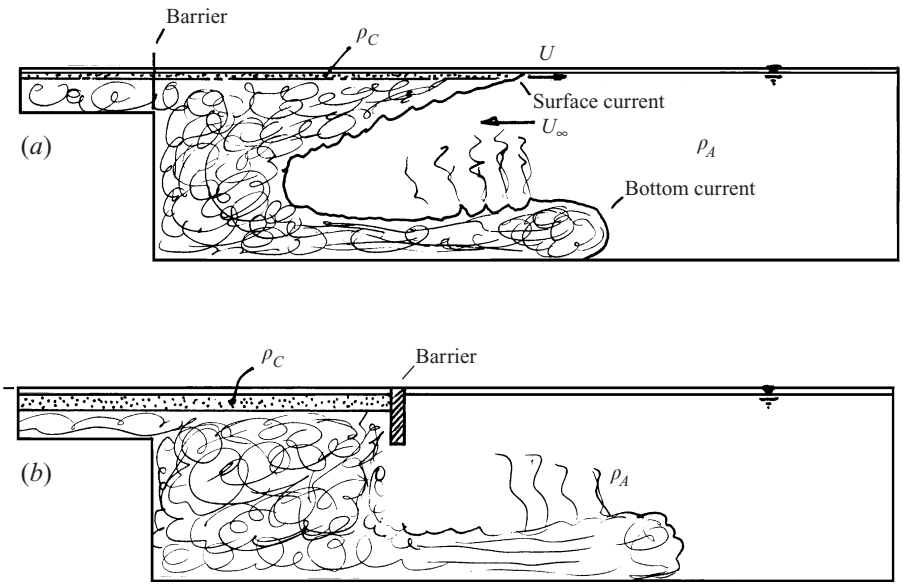

FIGURE 1. (*a*) Apparatus to study the evolution of a sedimenting, surface gravity current. The mixture of water and particles is initially retained behind the left-hand barrier. (*b*) The apparatus of (*a*) modified to study the flux of particles and water through the interface between them and the lower, heavier fluid.

secondary box was given a final, thorough stirring and the end barrier removed within one to two seconds, i.e. before any substantial sedimentation could take place to the bottom of the box. The motion of the current was recorded on video tape, and sometimes on photographic film, to be analysed later. An extensive series of experiments was run using combinations of two values of the lower-layer density ($\rho_A = 1.0380 \pm 0.0005$ and $1.0170 \pm 0.0005\,\mathrm{g\,cm^{-3}}$), one value of lock height (7.9 cm) and three values of its length (7.62, 15.24 and 22.86 ± 0.02 cm). For each combination between four and fourteen values of ρ_C were used, depending on the purpose of the particular sequence.

2.2. *Modified apparatus to study interface fluxes*

During the exploration of the parameter space outlined above it became clear that the forward motion of the current was being greatly modified by the flux of particles/interstitial fluid/ambient fluid through the interface. To study this phenomenon in more detail the tank used above was modified, as shown in figure 1(*b*). A barrier was placed 65 cm from the end of the tank so that, after the release of a particle/water mixture, the current was stopped by the barrier. After a few seconds a horizontally uniform layer of particles/water was formed. This layer was much thicker than that formed in the absence of the barrier and this improved the spatial resolution of the measurements described below.

Sedimentation began and when sufficient particles had entered the lower fluid to generate an unstable, intermediate layer large-scale convection began. The system was allowed to run until all of the particles had settled to the bottom of the tank. As before, a gravity current of particles and light mixed fluid traversed the bottom of the tank and into the right-hand compartment where the mixed fluid was eventually released as the particles sedimented to the bottom boundary. Samples were withdrawn

https://doi.org/10.1017/S002211209900556X Published online by Cambridge University Press

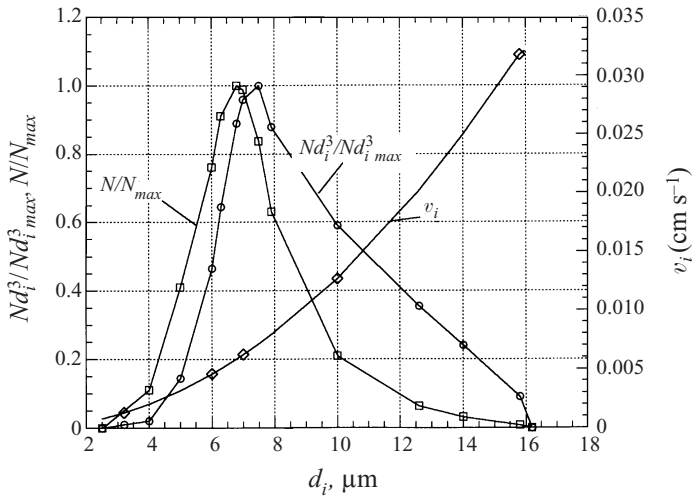

FIGURE 2. Normalized particle number (N/N_{max}), mass (Nd_i^3/Nd_{imax}^3) and Stokes settling velocity (v_i) as functions of particle diameter, d_i.

from various levels in the upper half of the tank using a specially designed, flattened nozzle that reduced contamination from fluid at other levels. The sample densities were measured to five decimal places using a 100 cm^3 specific gravity bottle. From these measurements the total density deficit could be found, compared with the initial deficit and the amount of interstitial fluid mixed into the lower layer calculated. Details of this calculation and the results therefrom are given in § 3.4.

3. Results and flow modelling for the release of a constant volume of particles/interstial fluid

3.1. *Dimensionless parameters*

The independent variables in this section of the work are: (*a*) the length (x_0) and height (h_0) of the initial reservoir of particles and pure water; (*b*) the densities of (i) the lower, ambient, fluid (ρ_A), (ii) the interstitial fluid (ρ_I), (iii) the upper layer of particles/water (ρ_C) and (iv) the particles themselves (ρ_P).

The particles are characterized by their normalized number (N/N_{max}) and weight [$Nd^3/(Nd^3)_{max}$] distributions with diameter (d_i) as shown in figure 2. Associated with each particle diameter is a free settling velocity (v_i) which we assumed is given by a balance between the particle buoyancy and the Stokes drag, so that

$$v_i = d_i^2\, g(\rho_P - \rho_I)/18\rho_I \nu_I, \tag{3}$$

where g is the acceleration due to gravity and ν_I the kinematic viscosity of water. Values of v_i for the particles used here are given on figure 2 also. In what follows we use a representative value of v_i to describe the whole distribution. This value, designated v_s is the velocity of the particles at the peak of the number distribution, i.e. with diameter 6.7 μm, with the result that $v_s/(g'h_0)^{1/2}$ becomes a further independent, dimensionless variable.

The measured, dependent variables are the position (x) of the front at time (t) after the removal of the barrier. Following Rottman & Simpson (1983), for example, we make x dimensionless with x_0 and t with $x_0/(g'h_0)^{1/2}$, where $g' = g(\rho_A - \rho_C)/\rho_A$.

https://doi.org/10.1017/S002211209900556X Published online by Cambridge University Press

In order to characterize the sedimentation process we make use of the formalism developed for double-diffusive phenomena (e.g. Turner 1976) and start by introducing the density-difference ratio:

$$R_\rho = (\rho_A - \rho_I)/(\rho_C - \rho_I). \tag{4}$$

In the present case this can vary from unity to large values, with the most intense convection occurring when R_ρ is close to unity. In what follows it is more useful to consider the quantity:

$$R = R_\rho - 1 = (\rho_A - \rho_C)/(\rho_C - \rho_I), \tag{5}$$

which now varies from zero to large positive values. Negative values represent layers that are gravitationally unstable even in the absence of sedimentation.

As will be seen the flux or mean velocity (V_i) of particles, plus interstitial fluid, through the interface is the physical quantity that is most important in determining how the motion of a gravity current, initially in a buoyancy–inertial balance, is modified by sedimentation. V_i has been measured during the initial stages of the current motion and is presented in dimensionless form in § 3.3.2 using both v_s and $(g'h_0)^{1/2}$ as reference velocities.

Note also that the largest value of c used here is approximately 0.04. This corresponds to a volume fraction of particles of about 0.013, a value that is considered to give particle dynamics that are minimally affected by particle/particle interactions (e.g. Davis & Acrivos 1985).

3.2. *Overall features of the flow*

3.2.1. *Typical flow evolution*

The two density differences between the ambient and interstitial fluids used here are $(\rho_A - \rho_I)/\rho_I = 0.0380 \pm 0.0005$ and 0.0170 ± 0.0005 and the corresponding values of the buoyancy jump in fluid properties across the interface, $\Delta g' = g(\rho_A - \rho_I)/\rho_I$ are $\Delta g'_1 = 37.3 \pm 0.5$ and $\Delta g'_2 = 16.7 \pm 0.5$. For these values and values of R greater than approximately 2, the motion of the current was not much different from the non-sedimenting case, and a further description is unnecessary. For values less than 2 and greater than approximately 0.15 the basic evolution of the current, with time, was the same except that the typical evolutionary time scale was shorter as R approached the smaller value. Here we describe a typical flow evolution for an intermediate case with $R = 0.77$.

A sequence of photographs for this case is shown in figure 3. The dark material is a mixture of fluid and black carborundum powder, although dye was often added to the released fluid in order to mark it when all the particles had sedimented out. Upon release of the dammed-up mixture its leading edge accelerated to a constant velocity (U_g) within the first 10–15 cm of travel. The constant-velocity phase (figure 3*a*) lasted until the current had travelled approximately 130 cm (figure 3*b*). At this time the current began to decelerate until it stopped at $x \approx 180$ cm. During this latter motion a sequence of strong convective plumes, that contained particles and a mixture of the interstitial and lower fluid, had developed below the surface current (figure 3*c–i*). Eventually (figure 3*f*) the plume nearest the nose became so energetic that it created a backflow that, as we shall see, was mainly responsible for the stopping of the primary current. While stopped the current continued to deposit particles until the interfacial flux was so small, and the density difference between the current and its surroundings so large, that the backflow was no longer able to stop its forward motion and it began to move forward again (figure 3*j*). This photograph shows, also,

https://doi.org/10.1017/S002211209900556X Published online by Cambridge University Press

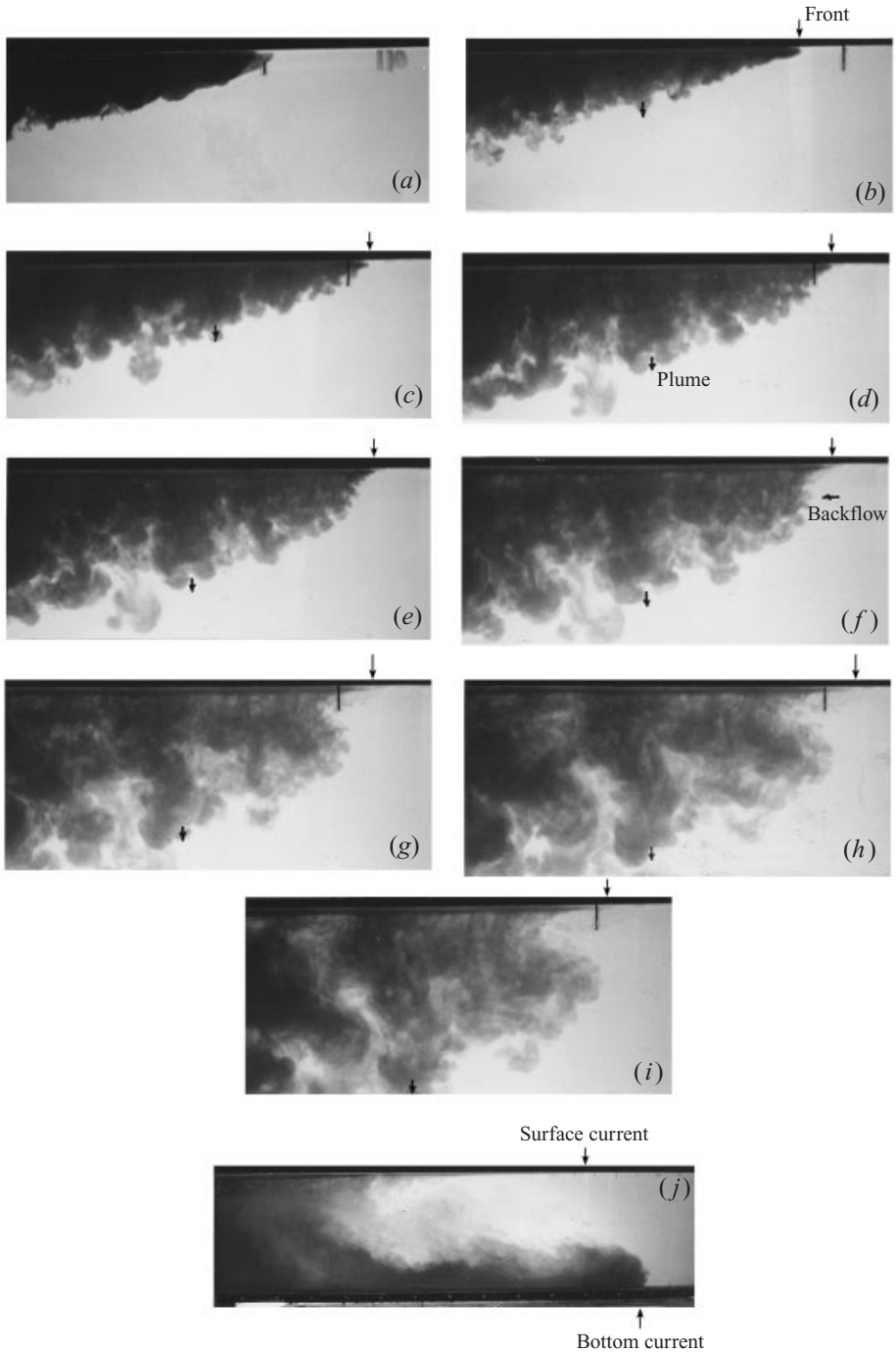

FIGURE 3 (*a–j*). Photographs of the time evolution of a sedimenting current for $R = 0.77$, $h_0 = 7.9$ cm, $x_0 = 15.24$ cm and $\Delta g_1' = 37.3$. Critically, at the time (*f*) was taken, a backflow generated by the convection to the left had developed. This flow, when inverted, is similar to the initial development of a sea-breeze front.

https://doi.org/10.1017/S002211209900556X Published online by Cambridge University Press

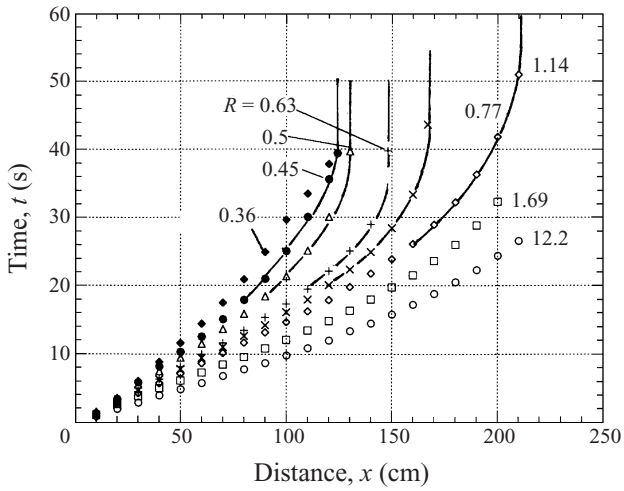

FIGURE 4. Raw data curves of the distance travelled by the nose of the current versus time. For the indicated values of R and $h_0 = 7.9\,\text{cm}$, $x_0 = 15.24\,\text{cm}$ and $\Delta g_1' = 37.3$.

that the mixture of particles and interstitial and ambient fluids that had reached the bottom of the tank formed a secondary gravity current that moved slowly along the bottom, and it too generated a backflow at the level of the primary current. The secondary current was of the type discussed by Sparks *et al.* (1993), in that it contained particles plus a fluid mixture that was lighter than the surroundings. In this case, as the particles sedimented to the bottom this lighter fluid was released to form upward-moving plumes that also contained some particles.

The exceptions to the description given above occurred when R was less than approximately 0.15. In these cases the rapid fallout of particles/interstitial fluid from the current, and the formation of a single, large plume, led to the very rapid evolution of the bottom gravity current. What was left of the virtually particle-free primary current was then able to 'escape' the influence of this evolution and was not stopped as its less energetic counterparts had been, at larger values of R.

In what follows we first quantify the statements made above, concerning the current motion, and then analyse and model each segment in an attempt to show the important dynamical balances that are responsible for each phase of this motion.

3.2.2. *Dimensionless x vs. t evolution, for various release volumes and values of R and ρ_A/ρ_I*

In figure 4 we show one example of the raw x vs. t data that have been obtained for a constant density difference $[(\rho_A - \rho_I)/\rho_I]$ of $0.0375\,\text{g cm}^{-3}$, with $h_0 = 7.9\,\text{cm}$ and $x_0 = 15.2\,\text{cm}$ and various values of R. Here one can see the effect of the decrease in $(\rho_A - \rho_C)$ on the initial velocity of the current and the asymptotic position of the front ($x_{equil.}$) as R decreases. As discussed above, these results should be made dimensionless using x_0 and $x_0/(g'h_0)^{1/2}$ as length and time scales respectively. Typical results are shown in figure 5 for the same conditions as figure 4 as well as some of the other cases that were run. Note that the behaviour after the 'asymptotic or equilibrium' length has been reached is not plotted because it was very difficult to extract from the video record due to both its small vertical scale and its lack of contrast with the background.

Several points are particularly noteworthy: (i) At large values of R the initial,

https://doi.org/10.1017/S002211209900556X Published online by Cambridge University Press

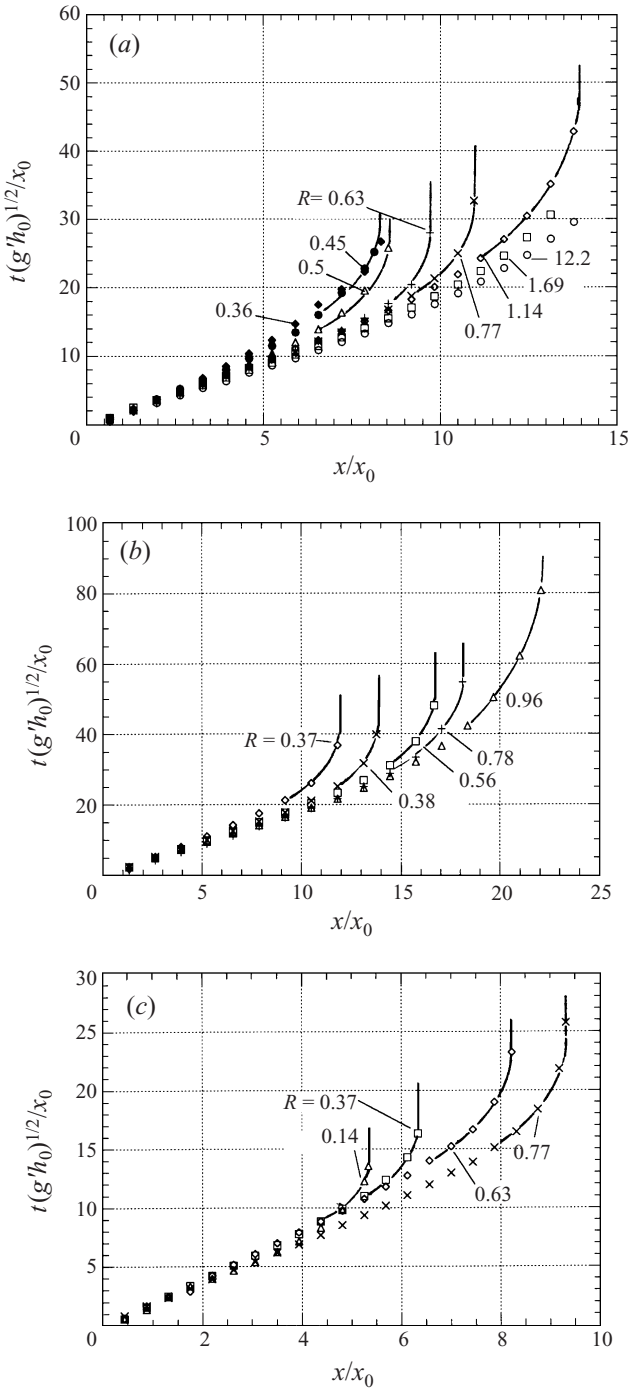

FIGURE 5. (*a*) The data of figure 4 normalized by the length scale, x_0, and time scale, $(g'h_0)^{1/2}/x_0$. (*b*) Normalized data for $h_0 = 7.9\,\text{cm}$ and $x_0 = 7.62\,\text{cm}$. (*c*) Normalized data for $h_0 = 7.9\,\text{cm}$ and $x_0 = 22.86\,\text{cm}$. All for $\Delta g_1' = 37.3$.

https://doi.org/10.1017/S002211209900556X Published online by Cambridge University Press

constant-velocity phase of the motion has a magnitude that agrees very closely with the results of Rottman & Simpson (1983) for the present experimental value of $h_0/H = 0.14$, i.e. $U_g = 0.63\ (g'h_0)^{1/2}$† (here H is the total depth of the tank). This implies that the current motion is not affected by sedimentation at these large values of R. (ii) As R decreases the initial velocity becomes smaller than the value given above. Here sedimentation is affecting the motion. (iii) The asymptotic length of the current, before it begins to move forward again, decreases as R decreases.

Two other quantities were measured, the first from the video record and the second by visual observation. These were the depth (h_F) of the convective plumes beneath the current versus time at a particular x location, and the time (t_c) taken between the passage of the head of the current and the beginning of convection from the underside of the current. These results will be presented later and in Maxworthy (2000) when they are needed to explain and/or motivate a particular point.

3.3. *Flow modelling and experimental interpretation*

3.3.1. *Introduction*

In the subsections that follow the experimental results introduced above will be dissected and each segment modelled in a way that appears to produce a self-consistent dynamical picture. In part we rely on a modelling effort that was reasonably successful in describing the dynamics of double-diffusive gravity currents (Maxworthy 1983). In particular it relies on the idea that the vertical transport of particles and interstitial fluid across the interface, between the current and its surroundings, takes with it the along-channel momentum of those same fluid elements which is then reduced to zero by interaction with the lower fluid. As a result the current experiences an effective surface stress equal to

$$\rho_C U V_i, \tag{6}$$

where U and V_i are the relevent along-channel and sedimentation velocities respectively, and the exact values of which depend on the segment of the motion being considered.

3.3.2. *Behaviour at early times*

The behaviour at early times can be simply characterized as a reduction of the constant velocity of propagation, under conventional buoyancy–inertia balance, by the flux of material through the interface at the head of the current. In this non-self-similar phase of the motion the horizontal force balance of the former, non-sedimenting flow, can be modelled as

$$k^{-2} h_0 U_g^2 \approx g' h_0^2 \tag{7}$$

where U_g is the velocity of the head of the gravity current with no sedimentation, and k^{-2} is an overall constant which combines both the relationship between the actual height of the current and h_0 and a measure of the effective drag on the head. Previous experiments have shown that for the value of h_0/H used here $k \approx 0.63$ (Rottman & Simpson 1983). Thus (7) gives

$$U_g = k(g'h_0)^{1/2}. \tag{8}$$

The effect of sedimentation is to modify (7), in the light of (6), to read

$$k^{-2} h_0 U_P^2 \approx g' h_0^2 - \kappa h_0 U_P V_i \tag{9}$$

† According to the experiments of Rottman & Simpson (1983) k is virtually constant at this value over the range of h_0/H from zero to 0.2.

https://doi.org/10.1017/S002211209900556X Published online by Cambridge University Press

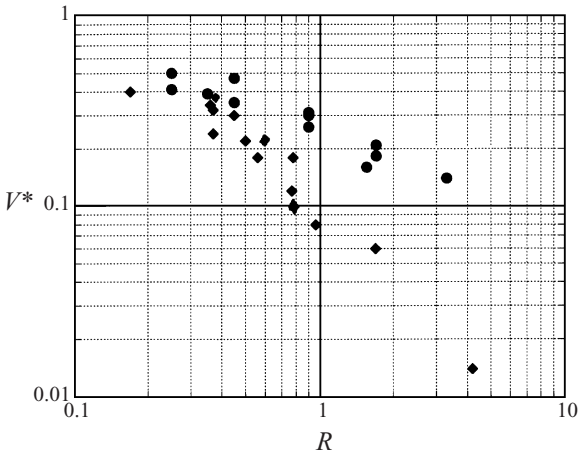

FIGURE 6. The effective sedimentation velocity through the interface made dimensionless with $(g'h_0)^{1/2}$, i.e. (V^*), versus R. For $\Delta g'_1 = 37.3$ (circles), $\Delta g'_2 = 16.7$ (diamonds) and all values of x_0.

where κ is a constant which relates the effective length of the gravity current head to h_0, and U_P is the velocity of the current with sedimentation.

Thus (9) can be manipulated to give

$$U_P/k(g'h_0)^{1/2} = -V^* \pm [V^{*2} + 1]^{1/2}, \tag{10}$$

where $V^* = (k\kappa V_i/2)/(g'h_0)^{1/2}$. Physically it only makes sense to use the plus sign in this equation, so that upon plotting the function V^* on the right-hand side of equation (10), one finds that, to a very good approximation

$$U_P/(g'h_0)^{1/2} \approx k(1 - 0.85V^*) \tag{11}$$

over the range of V^* of interest. Finally, it is more accurate, experimentally, to subtract the actual value of $U_g = k(g'h_0)^{1/2}$ found in these experiments for the case at the largest value of R, so that V^* is calculated from

$$V^* = (U_g - U_P)/0.85k(g'h_0)^{1/2}. \tag{12}$$

Thus $V_E = (k\kappa V_i/2) = V^*(g'h_0)^{1/2}$ represents an effective, average velocity of sedimentation through the interface, over the effective length of the current head, and furthermore its magnitude can be extracted from the experimental data. From figure 5, and similar ones for other sets of conditions, one can measure $U_P/(g'h_0)^{1/2}$ for each experiment and the reference value $U_g/(g'h_0)^{1/2}$ and hence calculate V^*, using (12) and the value of k (equal to 0.625) typical of these experiments. These results, for the two values of $\Delta g'$ used here, are shown in figure 6. As could have been anticipated, V^* is small for the larger values of R and increases rapidly as R approaches zero, and, significantly, depends, also, on $\Delta g'$.

This last result shows that R is not the only parameter to affect V^* but that, for a given value of R, V^* apparently also depends on the absolute magnitude of $(g'h_0)^{1/2}$. In an attempt to unravel this dependence the data of figure 6 were replotted as V_E/v_s, i.e. V^* multiplied by the dimensionless velocity ratio $(g'h_0)^{1/2}/v_s$, where v_s is a representative value of the fall velocity of the particles. In this case the velocity of the 6.7 μm particles was chosen (i.e. the particles at the maximum of the number distribution, figure 2), the numerical value of v_s being 0.006 cm s^{-1}. The resultant curves are plotted on figure 7. Here we find the interesting result that as R tends to

https://doi.org/10.1017/S002211209900556X Published online by Cambridge University Press

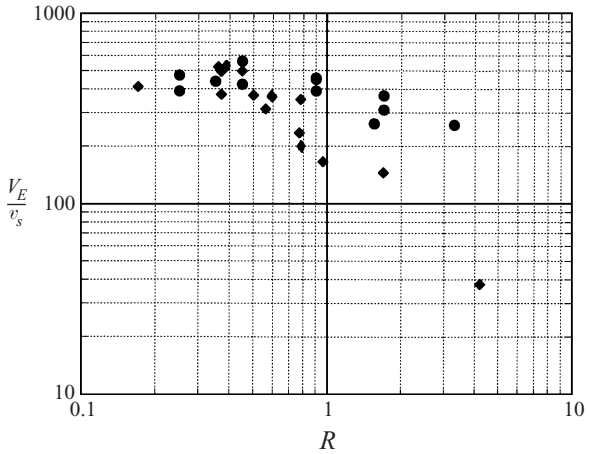

FIGURE 7. The effective sedimentation velocity (V_E) made dimensionless with the sedimentation velocity (v_s) of the 6.7 μm particles versus R. For the same two values of $\Delta g'_{1,2}$ as in figure 6 and all values of x_0.

zero V_E/v_s tends to a constant value of approximately 460, independent of the value of $\Delta g'$, but that $(g'h_0)^{1/2}/v_s$ is not sufficient to reduce the results for $R > 0.6$ to a single curve. The result above then gives a value for V_E of about $2.8 \pm 0.6\,\mathrm{cm\,s^{-1}}$ which is typical of the velocity in the plumes that fall from the underside of the current. A representative example is shown in figure 3 for a value of $R = 0.77$. Here the velocity of the current nose is $7.7\,\mathrm{cm\,s^{-1}}$ at a value of x around 100 cm, the angle of the plume front to the horizontal is $20 \pm 2°$, so that an average vertical velocity of the front of the plume cloud is roughly $2.8 \pm 0.3\,\mathrm{cm\,s^{-1}}$, in surprisingly good agreement with the value calculated above. For values of R greater than approximately 0.6 a dependence on $\Delta g'$ appears again.

This suggests the following interpretation. For values of R less than 0.6 the flux through the interface is so large that the forward motion of the head of the current has little effect upon it. However for larger values of R the translation of the head modifies the flux, presumably by a mechanism that involves the shear, and turbulence, at the interface. Thus for the larger value of $\Delta g'$ the flux is reduced far more than for the case of the smaller density ratio, i.e. where the values of $(g'h_0)^{1/2}$ are much smaller as well.

It is possible to collapse the data in a satisfactory way for the two values of $\Delta g'$ by using $R\Delta g'_{1,2}$ as abscissa. This result is shown, normalized by $\Delta g'_2$, in figure 8. Exactly why such a scaling works in this case is an open question but must be related to the arguments given above in a way that is not amenable to simple modelling at this time.

3.3.3. *Behaviour at intermediate and long times*

Towards the end of and after the constant-velocity phase discussed above the characteristic bulbous shape of the head disappeared and it took on a wedge-like, self-similar aspect. At the same time the velocity began to decrease, to eventually approach zero. It is possible to model at least two segments of this transition by making use of the results of Maxworthy (1983). In the first we consider the flow to be self-similar with the dynamical balance given by

$$g'h^2 \approx UV_sL, \tag{13}$$

https://doi.org/10.1017/S002211209900556X Published online by Cambridge University Press

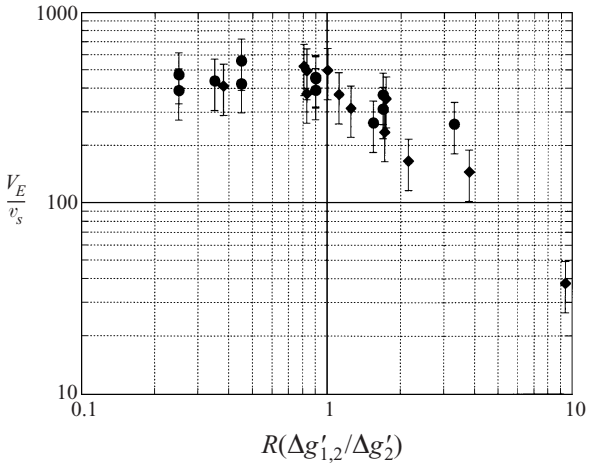

FIGURE 8. The data of figure 7 with the abscissa scaled as $R(\Delta g'_{1,2}/\Delta g'_2)$.

where L is the length and h a representative height of the current, and V_s a measure of the vertical velocity due to sedimentation in this case. Upon making use of the fact that $Lh \approx h_0 x_0 = A_0$, the volume of the current/unit width, and $U \approx L/t$ (i.e. U is now representative of the velocity of the whole current not just the head), one obtains the spreading law

$$L \approx [g' A_0^2 / V_s]^{1/4} t^{1/4}. \tag{14}$$

Here we have assumed, for small R, that the well-known balances for non-sedimenting currents i.e. between buoyancy and either inertia or viscous forces, are overwhelmed by the dominance of the force due to sedimentation (6). Clearly this may not be true for larger values of R and in these cases one can formally derive transition times between the three possible self-similar balances with buoyancy (inertial, with $L \approx t^{2/3}$; sedimenting, with $L \approx t^{1/4}$; and viscous, with $L \approx t^{1/5}$), as in Huppert (1982). However, in the present experiments the interesting dynamics were in the range of small R where these effects were not thought to be important.

In an attempt to describe the final stage of development, i.e. the existence of a current of constant length, we explore the consequences of a flow external to the current interacting with the flux of sediment. Quoting the equivalent result from Maxworthy (1983) we find for the buoyancy–sedimentation force balance

$$g' h^2 \approx U_0 V_s L, \tag{15a}$$

which gives

$$L \approx [g' A_0^2 / U_0 V_s]^{1/3} = \text{constant}, \tag{15b}$$

where U_0 is the external flow velocity imposed by either or both the backflow generated by the motion of the bottom, secondary, gravity current and the evolution of the leading edge of the sedimenting plume, as discussed above, and as will be expanded upon below. Note that in this case the flux due to sedimentation (V_s) must be from the exterior fluid into the upper layer. That this is possible is emphasized by the results of § 3.4 where this mixing of exterior fluid into the upper layer is clearly demonstrated. Thus (15*b*) indicates that the combination of a flux through the interface and an opposing, external flow is capable of stopping the motion of the

https://doi.org/10.1017/S002211209900556X Published online by Cambridge University Press

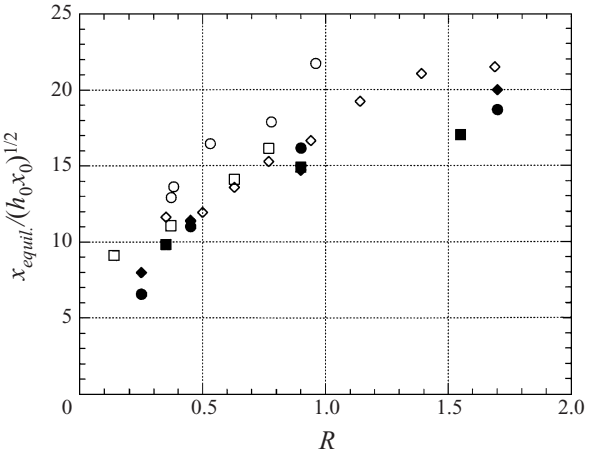

FIGURE 9. The asymptotic length of the current ($x_{equil.}$) scaled with $(x_0h_0)^{1/2}$ versus R. The filled points are for $\Delta g'_2 = 16.7$ and the open points for $\Delta g'_1 = 37.3$. All values of x_0.

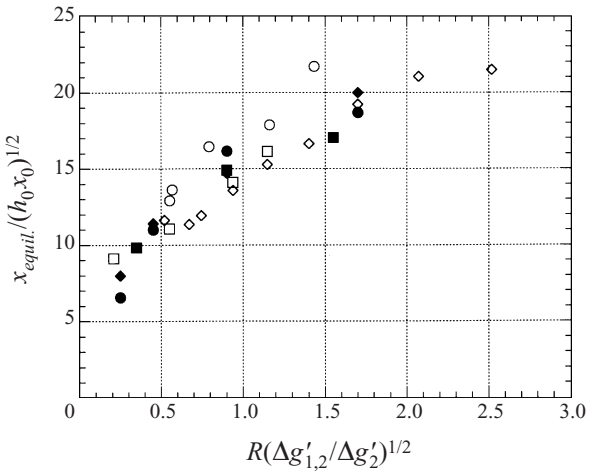

FIGURE 10. The data of figure 9 with the abscissa scaled as $R(\Delta g'_{1,2}/\Delta g'_2)^{1/2}$.

current. Also, even if an external flow exists it will not be effective in slowing the current if V_E is small or zero, as it is at the later stages of the motion, after most of the particles have sedimented out of the current.

In figure 9 we show measurements of $x_{equil.}/(x_0h_0)^{1/2}$ for most of the experiments performed during this study, where $x_{equil.}$ is the length of the current when its forward motion first stops. As can be seen, such a scaling is reasonably successful in collapsing the equilibrium length for each value of $\Delta g'$. A weak dependence on this parameter still exists. By scaling R as $R\,(\Delta g'_{1,2}/\Delta g'_2)^{1/2}$ it is possible to reduce the two curves to one (figure 10). As with the case of the sedimentation velocity there is no way to rationalize this result at this time. Even though equation (15*b*) gives a possible dependence on the parameters of the problem it contains at least one dependent variable that is difficult, if not impossible, to evaluate at this stage. Thus, U_0 depends on the opposing flow

https://doi.org/10.1017/S002211209900556X Published online by Cambridge University Press

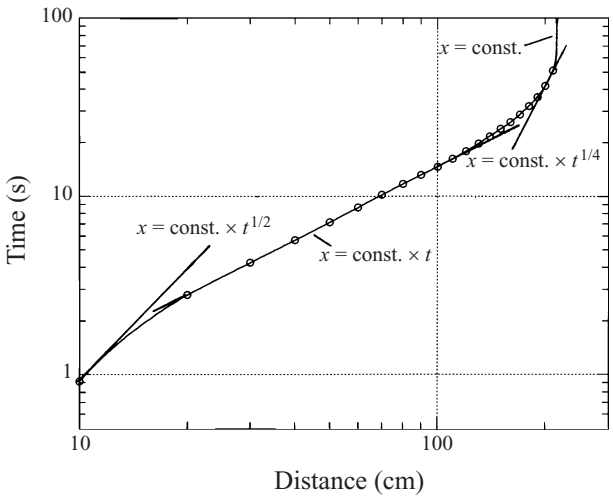

FIGURE 11. Time versus distance for $R = 1.14$, showing the various regimes of power-law behaviour.

generated by both the secondary gravity current and convection from the primary current. Its parametric dependence on the independent variables cannot be found from the simple experiments presented here. More extensive experiments are needed to explore this problems in more detail.

Based on the material presented in the two previous subsections the following scenario for the evolution of a sedimenting gravity current is proposed. We use the case for $R = 1.14$ and $x_0 = 15.4$ cm, shown on figure 11, as an example. This case gives a current that stops just before the end of the tank. Upon release of the initially stationary, well-mixed mass of particles and interstitial fluid the leading edge of the resultant current initially accelerates at a decreasing rate, with $x \approx t^{1/2}$, to a constant velocity, at $x \approx 20$ cm in figure 11. This sequence of events is typical of those found in similar cases, e.g. the acceleration of a region of mixed fluid in a stratified fluid (Amen & Maxworthy 1980). The constant front velocity is determined by a balance between the axial buoyancy difference and the sum of the drag force with no sedimentation and an interfacial stress due to the loss of axial momentum from the nose of the current. This phase of the motion is non-self-similar, as in a conventional current (Rottman & Simpson 1983). After the nose has travelled a certain distance ($x \approx 130$ cm on figure 11) it begins to decelerate and its shape slowly changes. During its transition from the constant-velocity state to that described by equation (13) inertia becomes less important and control changes from being at the nose to involving the whole current, i.e. the flow becomes self-similar, at approximately $x = 190$ cm. Equation (13) holds for only a short distance, to $x = 210$ cm. By that time the front velocity has become so small and the interfacial flux so large that a large plume, and associated induced velocity field, is formed (as in figure 3*f–j*). This field imposes an opposing velocity at the head of the current and its interaction with the interfacial flux slows the front further until it comes to rest, and equation (15*a*) then holds. This state exists for a while until the flux is reduced, and the buoyancy difference increased, enough for the current to start moving again, i.e. the left-hand side of equation (15*a*) then exceeds the right-hand side. This final stage most probably involves a viscous–buoyancy balance, with $x \approx t^{1/5}$.

https://doi.org/10.1017/S002211209900556X Published online by Cambridge University Press

3.4. *Late time characteristics and the fluxes of particles and upper-layer fluid*

As can be seen in the photographs of figure 3 after the gravity current front has passed a given location the instability commences and a sequence of plumes, consisting of a mixture of particles and upper- and lower-layer fluids, penetrates downwards. One can plot the vertical position of the front of these plumes, at a particular value of x, as a function of time in order to determine a measure of the temporal behaviour of the flux. Thus assuming that the buoyancy flux (B) has a temporal behaviour:

$$B \approx t^{\beta},$$

then the front should penetrate as

$$h_F \approx t^{3/2+\beta/2} = t^{\alpha}.$$

This is a modified version of the result of Fernado, Chen & Boyer (1994) which gives, for a constant buoyancy flux, $h_F \approx t^{3/2}$, where h_F is the depth of the front of the plumes below their initial position, i.e. before convection started.

As can be seen from figure 3 the interface between the convecting mixture of particles and fluid was very irregular, being made up of a number of large individual plumes. This made it very difficult to determine its vertical position (h_F), at any one x-location, as a function of time, in order to compare with the equation quoted above. A number of cases were analyzed and the data scatter was very large, so that no quantitative statements can be made about the value of α. The best one can say, qualitatively, is that α varied between 1 and something close to 1.5 as R varied from small to large values. This suggests that, in general, β was negative with a magnitude of order unity for the smaller values of R and approached zero for the larger values. Clearly this problem needs to be studied in more detail in the future, with better and more complete instrumentation.

To quantify this effect more thoroughly, and in a way that avoided the measurement of the frontal position, the apparatus of § 2.2 was used. Here a constant volume of particles and water was released in the horizontally constrained region between the source and the barrier shown in figure 1(*b*). A gravity current was generated which impacted the barrier so that after a few seconds a thick, uniform layer of particles and fluid was formed. Sedimentation began when the particles had invaded the lower, salty layer and formed a dense intermediate layer, as described above. The system was allowed to run-down until all the particles had settled to the bottom of the tank. As before, a gravity current of particles and mixed fluid moved along the bottom of the tank into the right-hand compartment where the mixed fluid was released, away from the original layer. As described in § 2.2, samples were taken from various depths within this layer using a flattened nozzle and sample densities were measured to five decimal places. A typical result is shown in figure 12. From these data the density deficit

$$\int [\rho_A - \rho(y)]\mathrm{d}y$$

could be found and compared with the initial deficit

$$[\rho_A - \rho_I]\Delta.$$

Where Δ is the initial thickness of the upper layer, and we have assumed that the initial density distribution is of the two-layer type. Subtracting these two results and dividing by $[\rho_A - \rho_I]$ gives the depth (δ) of upper-layer fluid lost to the lower layer:

https://doi.org/10.1017/S002211209900556X Published online by Cambridge University Press

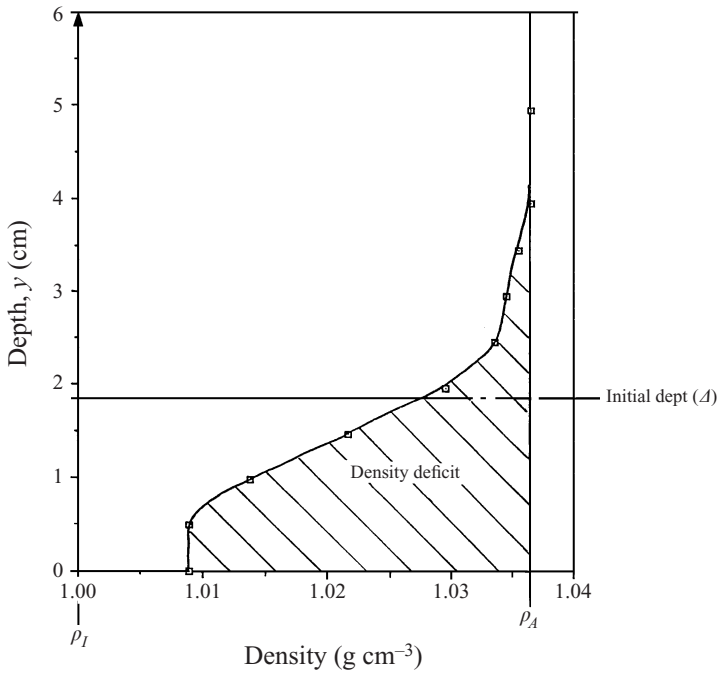

FIGURE 12. Density versus depth after the sedimentation of all the particles through a stratified interface. The density deficit used in the calculations in the figure and text is shaded. Note that the depth from the surface is plotted as the positive ordinate.

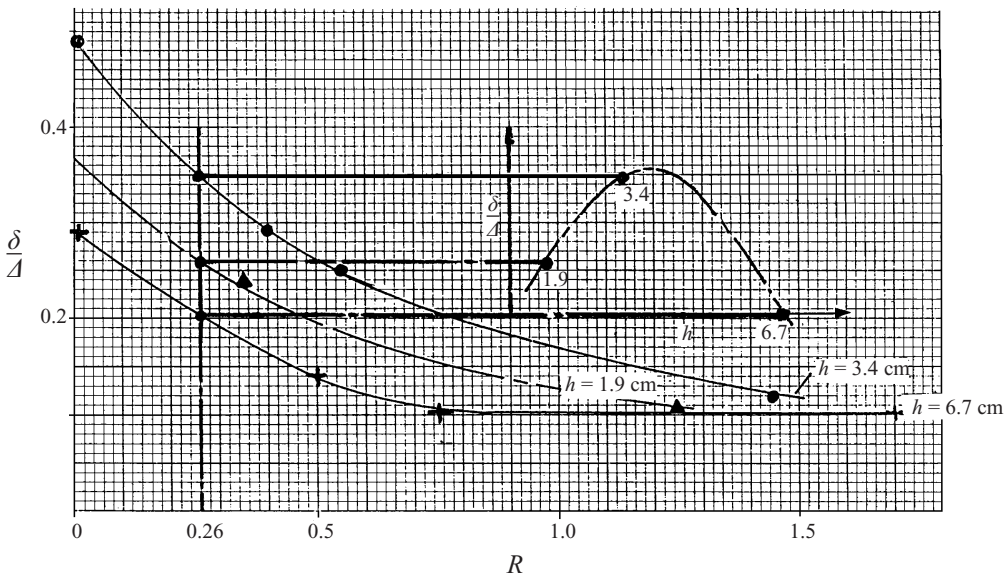

FIGURE 13. The amount of upper-layer fluid transported and mixed into the lower layer by particle sedimentation through the interface versus R, for three values of the initial layer depth (h). The insert shows a cross-plot of δ/Δ versus h for $R = 0.26$, indicating the existence of a value of h at which δ/Δ is a maximum.

https://doi.org/10.1017/S002211209900556X Published online by Cambridge University Press

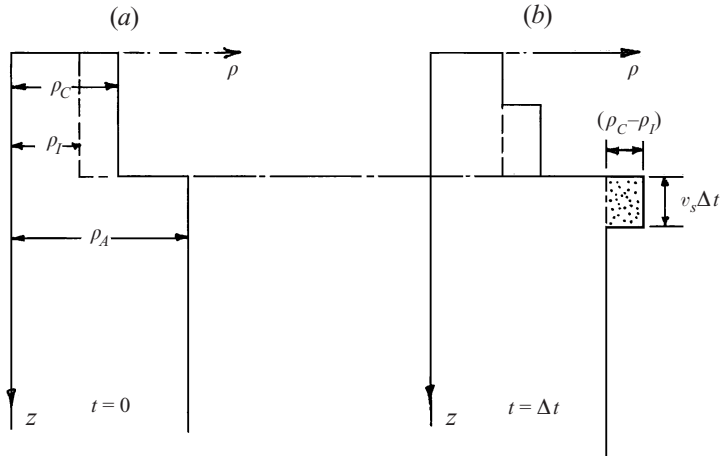

FIGURE 14. Schematic of the processes leading to the instability of a sedimenting front in the simplest case of a thin interface and monodisperse particle distribution. (*a*) Initially the two layers are stable. (*b*) After a short time a layer of particles has sedimented into the lower layer to form a gravitational unstable system.

$$\delta = \Delta - \int \{[\rho_A - \rho(y)]/[\rho_A - \rho_I]\} \mathrm{d}y.$$

A number of experiments with different values of R and initial fluid depths were carried out. The results are summarized in figure 13. As expected the loss of interstitial fluid is greater as R tends to zero and clearly there is an optimum value of the fluid depth between 3.4 and 6.7 cm (shown in the inset to the figure). The total loss can be substantial, with up to 50 % of the interstitial fluid mixing downwards in the most extreme case. Also note that the minimum density ($\rho \approx 1.009\,\mathrm{g\,cm^{-3}}$) in figure 13 is greater than the initial density ($\rho \approx 1.000\,\mathrm{g\,cm^{-3}}$) of the upper layer. This indicates that lower-layer fluid has also mixed upwards during the sedimentation process, cf. double-diffusive convection. Unfortunately such measurements only give the overall mixing due to sedimentation not the temporal variation of the mixing rate or flux, which is needed for the modelling of § 3.3. The latter would require more sophisticated apparatus and instrumentation than used here.

4. Discussion and conclusions

It has been shown that the role of sedimentation from a surface gravity current is crucial to its motion when R is less than, approximately, 2. The passage of particles through the interface has several effects. First, it can result in an effective stress at the interface that can oppose the gravitational driving force. The convective plumes in the lower layer, that result from this sedimentation, can then induce an opposing external flow at the interface which, when it interacts with the interface flux, results in a force that can stop the forward motion of the current. When the convective plumes, which contain a mixture of particles and upper- and lower-layer fluid, reach the bottom of the tank they generate a secondary gravity current, the flow external to which can also interact with the interface flux to reinforce the force opposing the motion. Each of these opposing effects are very nonlinear functions of the independent variables and their detailed measurement is a suitable subject for future investigations.

Finally, the dynamical processes that lead to the instability of the sedimenting

https://doi.org/10.1017/S002211209900556X Published online by Cambridge University Press

front, the formation of frontal plumes and the rapid transfer of particles and the fluid across the interface is an important issue. The details are discussed in Maxworthy (2000), where simple models are proposed. In summary it appears that the growth of the observed frontal instability is controlled by the intrusion of a growing layer of buoyancy excess between two stable fluid layers, as represented in figure 14. Here, for simplicity, it is assumed that the interface between the two fluids in thin and that the sedimenting particles are monodisperse. While this appears, on the surface, to be a simple application, and extension, of the theories of Rayleigh–Taylor gravitational instability a number of complicating factors are present. As a result the presentation and discussion are contained in a separate paper (Maxworthy 2000).

The crucial role played by Professor H. E. Huppert, FRS, in obtaining funding from National Environmental Research Council of the UK, and during technical discussions, is acknowledged with profound thanks. The work was performed while I was a Senior Visitor at DAMTP, Cambridge, where the support, in the laboratory, of Drs P. F. Linden and S. Dalziel and Mr D. Cheesely eased the task of running the experiments and made my stay a very pleasant one. Discussions with Professors L. G. Redekopp of USC and G. Homsy of Stanford University as well as Dr J. Hinch of DAMTP are acknowledged with thanks also.

REFERENCES

Amen, R. & Maxworthy, T. 1980 The gravitational collapse of a mixed region into a linearly stratified fluid. *J. Fluid Mech.* **96**, 65–80.

Batchelor, G. K. & Nitsche, J. M. 1991 Instability of stationary stratified fluid. *J. Fluid Mech.* **227**, 357–391.

Bonnecaze, R. T., Huppert, H. E. & Lister, J. R. 1993 Particle-driven gravity currents. *J. Fluid Mech.* **250**, 339–369.

Chen, C. H. 1997 Particle transport through sedimenting fingers. *Deep-Sea Res.* (Submitted).

Davis, R. H. & Acrivos, A. 1985 Sedimentation of non-colloidal particles at low Reynolds numbers. *Ann. Rev. Fluid Mech.* **17**, 91–118.

Fernado, H. J. S., Chen, R.-R. & Boyer, D. L. 1994 Effects of rotation on convective turbulence. *J. Fluid Mech.* **228**, 513–547.

Green, T. 1987 The importance of double diffusion to the settling of suspended material. *Sedimentology* **34**, 319–331.

Huppert, H. E. 1982 The propagation of two-dimensional and axisymmetric viscous gravity currents over a rigid horizontal boundary. *J. Fluid Mech.* **121**, 43–58.

Maxworthy, T. 1983 The dynamics of double diffusive gravity currents. *J. Fluid Mech.* **128**, 259–282.

Maxworthy, T. 2000 The stability of a sedimenting, stratified front, *J. Fluid Mech.* (in preparation).

Rottman, J. W. & Simpson, J. E. 1983 Gravity currents produced by instantaneous releases of a heavy fluid in a rectangular channel. *J Fluid Mech.* **135**, 95–110.

Sparks, R. S. J., Bonnecaze, R. T., Huppert, H. E., Lister, J. R., Hallworth, M. A., Mader, H. & Phillips, J. 1993 Sediment-laden gravity currents with reversing buoyancy. *Earth Planet. Sci. Lett.* **114**, 243–257.

Turner, J. S. 1976 *Buoyancy Effects in Fluids.* Cambridge University Press.

https://doi.org/10.1017/S002211209900556X Published online by Cambridge University Press